

Structure and dielectric properties of polar fluids with extended dipoles: results from numerical simulations

V. BALLENEGGER* and J.-P. HANSEN

Department of Chemistry, University of Cambridge, Lensfield Road,
Cambridge CB2 1EW, UK

(Received 8 December 2003; revised version accepted 16 February 2004)

The strengths and shortcomings of the point dipole model for polar fluids of spherical molecules are illustrated by considering the physically more relevant case of extended dipoles formed by two opposite charges $\pm q$ separated by a distance d (dipole moment $\mu = qd$). Extensive molecular dynamics simulations on a high-density dipolar fluid are used to analyse the dependence of the pair structure, dielectric constant ϵ and dynamics as a function of the ratio d/σ (σ is the molecular diameter), for a fixed dipole moment μ . The point dipole model is found to agree well with the extended dipole model up to $d/\sigma \simeq 0.3$. Beyond that ratio, ϵ shows a non-trivial variation with d/σ . When $d/\sigma > 0.6$, a transition is observed towards a hexagonal columnar phase; the corresponding value of the dipole moment is found to be substantially lower than the value of the point dipole required to drive a similar transition.

1. Introduction

Highly polar fluids are particularly important in many areas of physical chemistry, chemical engineering and biology, because of their role as solvents leading to electrolyte and polyelectrolyte dissociation. Water is of course the most important among polar liquids, but because of its complex behaviour, primarily linked to the formation of hydrogen-bond networks, much theoretical work has focused on simpler models involving spherical molecules with point dipoles. The best known and most widely studied examples are dipolar hard spheres (DHS), dipolar soft spheres (DSS), and the Stockmayer model (dipolar + Lennard-Jones interactions). A long-standing problem, going back to the classic work of Onsager [1] and Kirkwood [2], is to relate the dielectric response of a polar fluid to molecular dipole fluctuations and correlations (for reviews, see [3]). Subtle conceptual and numerical problems arise in molecular dynamics or Monte Carlo simulations of finite samples of polar fluids, which are linked to the infinite range of the dipolar interactions, so that boundary conditions must be treated adequately. These issues were resolved in the early 1980s, for both the reaction field and the Ewald summation implementations of boundary-conditions [4–6]. Despite this theoretical progress, accurate estimates of the dielectric permittivity of simple polar fluids by numerical simulation remain a very challenging task, because large

fluctuations of the total dipole moment of the sample occur on a relatively long time scale (of the order of 10 ps), leading to a very slow convergence rate for the dielectric constant [7, 8] (see also §3).

More recently, it was realized that simple dipolar liquids can form a ferroelectric nematic phase for sufficiently large dipole moments [9–11]. This transition is intimately related to the formation of chains of dipoles aligned head-to-tail, which prevent the formation of a proper liquid phase in the Stockmayer model if the dispersive energy is below a certain threshold [12].

However, point dipoles represent a limiting situation, never achieved in real polar molecules, which are characterized by extended charge distributions linked to electronic charge transfer from electron donors to electron acceptor atoms. In simple heteronuclear diatomic molecules such as CO or HF, this situation can be modelled by assigning fractional charges of opposite sign to sites that are separated by a distance d , typically of the order of 0.1 nm [13]. Such situations, or more complicated ones involving more than two atoms, can be mimicked by adding higher-order point multipoles to a point dipole [14], but such an expansion will require more and more high-order multipoles as two molecules approach each other.

In this paper, we present a systematic investigation of the structure, dielectric response and phase behaviour of a simple model involving spherical molecules carrying extended (rather than point) dipoles resulting from opposite charges $\pm q$, each displaced symmetrically by

*Author for correspondence. e-mail: vcb25@cam.ac.uk

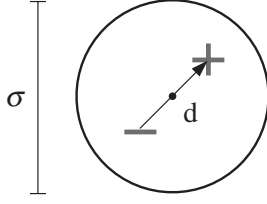


Figure 1. A polar molecule with an extended dipole moment.

a distance $d/2$ from the centre of the molecule. We study how the properties of the polar liquid change when d is increased from zero, varying q simultaneously so that the dipole moment $|\boldsymbol{\mu}| = qd$ remains constant. Although polar molecules are never spherical, the model investigated in this paper, which focuses on the electrostatic rather than steric interactions, is the simplest ‘natural’ extension of the dipolar sphere model towards a more realistic representation of highly polar fluids. Some studies on the structure of similar models with extended dipoles have been published previously, but without an investigation of their bulk dielectric properties [15, 16].

2. The model and simulation details

We consider a polar fluid made up of spherical molecules with two embedded point charges $\pm q$ located at $\pm \mathbf{d}/2$ from the centre of the sphere (see figure 1). The distance $|\mathbf{d}|$ is assumed fixed, so the molecule is not polarizable and carries a permanent dipole moment $\boldsymbol{\mu} = q\mathbf{d}$.

Placing the origin at the centre of the sphere, the multipole moments $q_{lm} = \int Y_{lm}^*(\theta, \phi) r^l \rho(\mathbf{r}) d^3\mathbf{r}$, where $\rho(\mathbf{r}) = q\delta(\mathbf{d}/2) - q\delta(-\mathbf{d}/2)$ is the molecular charge distribution [17], are

$$q_{lm} = \begin{cases} 2q \left(\frac{d}{2}\right)^l \sqrt{\frac{2l+1}{4\pi}} & \text{if } l \text{ odd and } m=0 \\ 0 & \text{otherwise.} \end{cases} \quad (1)$$

The next non-vanishing moment after the dipole is thus the octopole, since the quadrupole moment vanishes by symmetry for this choice of origin.

The interaction energy between two molecules is given by the sum of a Lennard-Jones interaction

$$V_{LJ}(r) = 4u \left[\left(\frac{\sigma}{r}\right)^{12} - \left(\frac{\sigma}{r}\right)^6 \right] \quad (2)$$

and the four Coulombic energies due to the point charges. On figure 2, the electrostatic energy at contact is compared to a truncated multipolar expansion containing the dipole–dipole and dipole–octopole interactions. The configuration of lowest energy occurs when the molecular dipoles are aligned head-to-tail

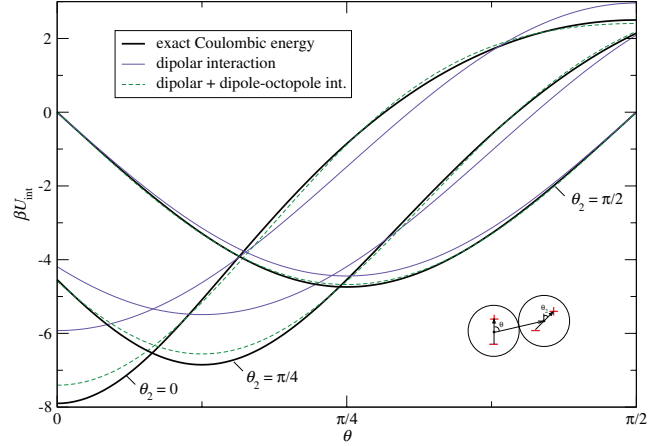


Figure 2. Electrostatic interaction energy of two molecules at contact ($|\mathbf{r}| = \sigma$) for $d = \sigma/2$.

($\theta = \theta_2 = 0$). This minimum energy is lower for extended than for point dipoles.

A thermodynamic state of the fluid is specified by the values of the dimensionless parameters:

- reduced density: $\rho^* = \rho\sigma^3$,
- reduced temperature: $T^* = kT/u$,
- reduced dipole moment: $\mu^* = \sqrt{\mu^2/\sigma^3u}$,
- reduced dipole elongation: $d^* = d/\sigma$.

We studied the influence of dipole elongation on properties of a dense highly polar fluid phase characterized by $\rho^* = 0.82$, $T^* = 1.15$, $\mu^* = 1.82$.[†] The reduced moment of inertia of our molecules was $I^* = I/m\sigma^2 = 0.117$, but equilibrium quantities, such as the dielectric constant and distribution functions, are independent of I^* . We also performed simulations of a dipolar *soft* sphere fluid at $\rho^* = 0.8$, $T^* = 1.35$ and $\mu^* = 2$. This thermodynamic state point of the DSS fluid has been extensively studied by Kusalik in the case of point dipoles [7, 18].

In all calculations, we employed periodic boundary conditions. We choose the spherical geometry, that is the periodic replications of the basic cubic simulation cell form an infinite sphere, which is itself embedded in an infinite region of dielectric constant ϵ' . In this case, the Hamiltonian of the system is

$$H = \sum_{i < j=1}^N (V_{LJ}(\mathbf{r}_{ij}) + q_i q_j \Psi(\mathbf{r}_{ij})) - \frac{\kappa}{\pi^{1/2}} \sum_{i=1}^N q_i^2 + \frac{2\pi \mathbf{M}^2}{(2\epsilon' + 1)L^3}, \quad (3)$$

[†] Our parameters in dimensioned units were $T = 300$ K, $\mu = 2.45$ D, $\sigma = 0.3668$ nm, $m = 10$ u, $I = 0.156$ u nm², $u = 2.1747$ kJ mol⁻¹.

Table 1. Influence of dipole elongation on some properties of a Stockmayer fluid at $\rho^* = 0.82$, $T^* = 1.15$ and $\mu^* = 1.82$.

d/σ	ϵ	τ_M (ps)	τ_μ (ps)	D (10^{-5} cm ² /s)	p^*	U^*
0.02	99.6(± 1.4)	2.21	0.50	11.7	0.42	-10.1
0.3	98.4(± 1.5)	2.64	0.54	11.6	0.45	-10.2
0.4	94.0(± 1.5)	2.88	0.63	11.5	0.45	-10.3
0.5	92.4(± 1.7)	4.14	0.88	10.6	0.42	-10.6
0.6	102.3(± 3.2)	11.44	2.01	8.7	0.26	-11.7
0.61	104.7(± 3.6)	13.97	2.36	8.5	0.23	-11.9
0.62	100.8(± 3.5)	14.81	2.79	7.9	0.19	-12.1

where L is the side of the box, $\mathbf{M} = \sum_i q_i \mathbf{r}_i$ is the total dipole moment, and

$$\Psi(\mathbf{r}) = \sum_{\mathbf{n} \in \mathbb{Z}^3} \frac{\text{erfc}(\kappa|\mathbf{r} + \mathbf{n}L|)}{|\mathbf{r} + \mathbf{n}L|} + \frac{1}{\pi L} \sum_{\mathbf{n} \neq 0} \frac{1}{|\mathbf{n}|^2} \exp\left(\frac{-\pi^2|\mathbf{n}|^2}{\kappa^2 L^2} + \frac{2\pi i}{L} \mathbf{n} \cdot \mathbf{r}\right). \quad (4)$$

The last term in (3) accounts for the work done against the depolarizing field created by surface charges induced on the spherical boundary. This term vanishes only for metallic boundary conditions ($\epsilon' = \infty$). The Ewald sums in $\Psi(\mathbf{r})$ were evaluated using the smooth particle mesh Ewald method [19] (Ewald coefficient $\kappa = 3.4705 \text{ nm}^{-1}$, grid size $32 \times 32 \times 32$, interpolation order 6). The interactions were truncated beyond 0.9 nm, both for the real space Ewald sum and for the Lennard-Jones interactions.

Molecular dynamics simulations were carried out using the simulation package *gromacs* [20]. The equations of motion were integrated using the so-called leap-frog algorithm with a reduced time step of $dt^* = dt/(m\sigma^2/u)^{1/2} = 0.0025$. The temperature was kept constant using a Berendsen thermostat. Equilibration periods lasted at least 100 ps (50 000 time steps), and were followed by data-producing runs of 8 ns or more. The number of molecules was 512 in calculations of the dielectric constant (§3), and 5555 in calculations of correlation functions (§4).

3. Dipole fluctuations and dielectric constant

The dielectric constant of a homogeneous and isotropic fluid can be calculated from the fluctuation formula (see, for example, [21])

$$\frac{(\epsilon - 1)(2\epsilon' + 1)}{2\epsilon' + \epsilon} = \frac{4\pi \langle \mathbf{M}^2 \rangle}{3V kT}, \quad (5)$$

which holds for a macroscopic spherical sample of volume V surrounded by a medium of dielectric constant ϵ' . The results obtained for the dielectric

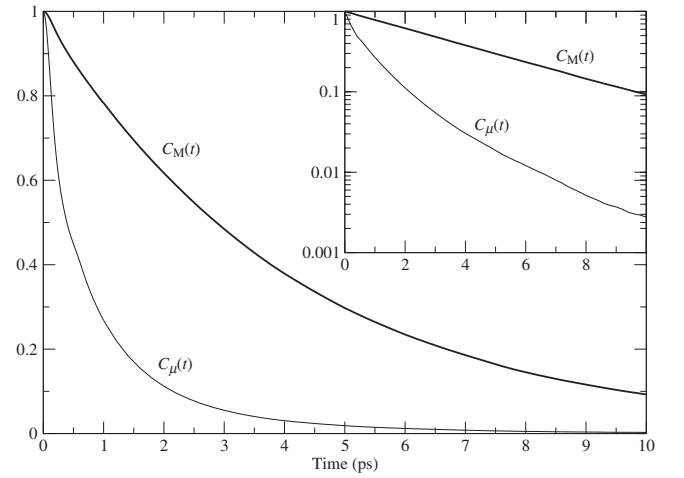


Figure 3. Autocorrelation functions $C_M(t)$ and $C_\mu(t)$, for the value $d = \sigma/2$. The inset shows a logarithmic plot, confirming the exponential behaviour of $C_M(t)$.

constant are independent of the choice of ϵ' , provided the boundary term in equation (3) is properly taken into account. We employed metallic boundary conditions, because they are known to produce smaller uncertainties in estimates of ϵ than finite values of ϵ' [5, 22] (see also below). The fluctuation formula reduces in this case to

$$\epsilon = 1 + 3y \langle g \rangle, \quad g = \frac{M^2}{N\mu^2}, \quad (6)$$

where the dimensionless parameter $y = 4\pi\beta\rho\mu^2/9 \simeq 3.31$ at the state point under consideration.

Table 1 shows the influence of the dipole elongation on some properties of the Stockmayer fluid, namely on the dielectric constant ϵ , the diffusion constant D , the dielectric relaxation times τ_M and τ_μ , the reduced configurational energy $U^* = U/(Nu)$, and the reduced pressure $p^* = p\sigma^3/u$. The diffusion constant was calculated from Einstein's relation

$$\langle |\mathbf{r}_i(t) - \mathbf{r}_i(0)|^2 \rangle = 6Dt, \quad t \rightarrow \infty. \quad (7)$$

The relaxation times τ_M and τ_μ were determined from the autocorrelation functions $C_M(t) = \langle \mathbf{M}(t) \cdot \mathbf{M}(0) \rangle /$

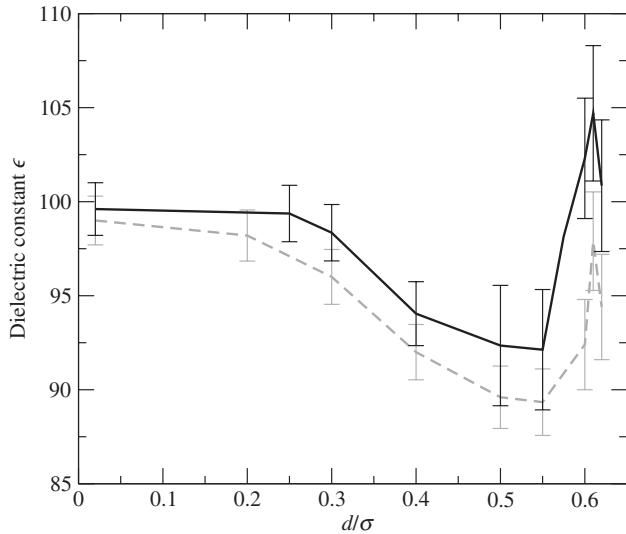


Figure 4. Dielectric constant of a Stockmayer fluid ($\rho^* = 0.82$, $T^* = 1.15$, $\mu^* = 1.82$, continuous line) and of a dipolar soft sphere fluid ($\rho^* = 0.8$, $T^* = 1.35$, $\mu^* = 2$, dashed line) as a function of dipole extension.

$\langle M^2 \rangle$ and $C_\mu(t)$ (see figure 3). For $t > 0.3$ ps, $C_M(t)$ exhibits an exponential decay $\exp(-t/\tau_M)$ typical of a Debye dielectric. The relaxation of $C_\mu(t)$ is not well fitted by a single exponential, and the corresponding relaxation time was estimated from the integral of $C_\mu(t)$.

We show in figure 4 the variation of the dielectric constant with dipole elongation for a Stockmayer fluid and for a dipolar soft sphere fluid. For almost point dipoles ($d^* = 0.02$), our result for the dielectric constant of the DSS fluid is in good agreement with the value 98 ± 2 reported by Kusalik *et al.* [23]. At the state point under consideration, the Stockmayer fluid has almost the same dielectric constant: $\epsilon_{\text{point}} = 99.6 \pm 1.4$. Our data show that when d^* increases, the dielectric constant decreases and reaches a minimum about 6% lower than ϵ_{point} at $d^* \simeq 0.55$. When d^* is further increased, the dielectric constant increases rapidly above ϵ_{point} , up to the critical distance $d_c^* \simeq 0.63$. At this critical distance, a phase transition occurs from an isotropic fluid to an orientationally ordered ‘liquid crystal’ phase (see § 5).

The simulations show that the point dipole model gives a reliable estimate of the dielectric constant over a very wide range of extensions d , namely up to the point where the system undergoes a phase transition. The weak sensitivity of the dielectric constant on the extension of the dipole, which contrasts with the large sensitivity observed in water models [24], may be due to the absence of a quadrupole moment in our molecules.

It is clear from table 1 that the dynamics of the fluid slows down when d is increased: the diffusion coefficient D drops and the relaxation times increase. This slow-down is due to the formation of head-to-tail dipolar

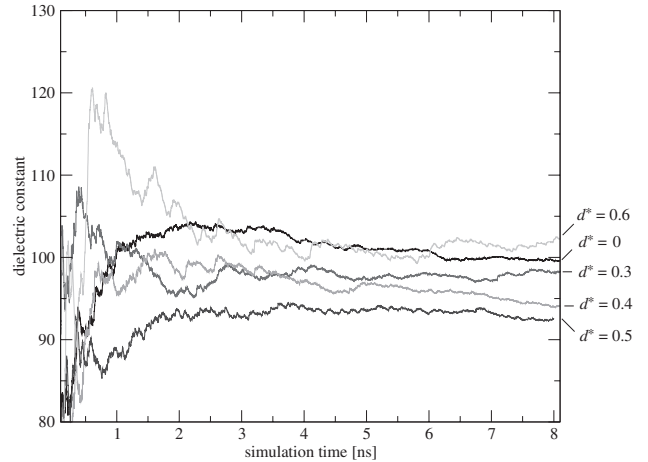


Figure 5. Convergence of ϵ with simulation time, for dipole elongations $d^* = d/\sigma = 0, 0.3, 0.4, 0.5$ and 0.6 .

chains in the system. Their entanglement makes these chains less mobile than individual molecules in the present high-density regime.

Long runs were needed to obtain even moderate accuracy (about 2%) in the estimated dielectric constants. Figure 5 shows the running estimate of ϵ as a function of simulation time. The slow convergence, especially for large elongations of the dipole, can be traced back to the long relaxation times τ_M , as shown by the following error analysis.

By definition, the probability distribution of the sample having a total dipole moment of magnitude M and arbitrary orientation is given by

$$P(M) \propto 4\pi M^2 e^{-\beta F(M)}, \quad (8)$$

where $F(M)$ is the free energy of the system. From macroscopic electrostatics, the energy of a spherical dielectric sample, of dielectric constant ϵ and carrying a uniform polarization M/V , is

$$U(M) = \frac{2\pi M^2}{V} \frac{2\epsilon' + \epsilon}{(\epsilon - 1)(2\epsilon' + 1)}, \quad (9)$$

where ϵ' is the dielectric constant of the surrounding medium. Following Kusalik [25], we combine equations (8) and (9) with the approximation $F(M) \simeq F(0) + U(M)$. This leads to the following expression for the probability distribution of fluctuations $g = M^2/(N\mu^2)$:

$$P(g) = Ag^{1/2} e^{-\kappa g}, \quad \kappa \equiv \frac{9y}{2} \frac{2\epsilon' + \epsilon}{(\epsilon - 1)(2\epsilon' + 1)}, \quad (10)$$

where the normalization constant is $A = 2(\kappa^3/\pi)^{1/2}$. The mean of this distribution is $\langle g \rangle = 3/(2\kappa)$, in agreement

with the fluctuation formula (5). Though the distribution (10) neglects changes in entropy and is valid only in the linear regime, it gives a good description of fluctuations of the total dipole moment observed in simulations of highly polar fluids [23].

The dielectric relaxation time τ_M gives a time scale for two measurements of M^2 to be independent. In a simulation of total duration t , the distribution (10) is thus sampled $n \simeq t/\tau_M$ times. After n such independent measurements, the standard deviation in the average $\sum_{i=1}^n g_i/n$ of the g factor is $\sigma_{g,n} = \sigma_g/n^{1/2}$ where $\sigma_g^2 = \langle (g - \langle g \rangle)^2 \rangle = 3/(2\kappa^2)$ is the variance of the distribution (10). The expected relative uncertainty in the g factor,

$$I_{\langle g \rangle} \equiv \frac{\sigma_{g,n}}{\langle g \rangle} = \sqrt{\frac{2}{3n}} = \sqrt{\frac{2}{3}} \frac{\tau_M}{t}, \quad (11)$$

depends therefore on the boundary condition ϵ' only via the relaxation time τ_M . Solving (5) for ϵ , one has

$$\epsilon - 1 = \frac{3y\langle g \rangle(2\epsilon' + 1)}{2\epsilon' + 1 - 3y\langle g \rangle}. \quad (12)$$

By the rules of propagation of errors, the relative uncertainty in the dielectric constant minus one is thus

$$I_{\epsilon-1} = \frac{2\epsilon' + \epsilon}{2\epsilon' + 1} \sqrt{\frac{2}{3}} \frac{\tau_M}{t}. \quad (13)$$

The error bars in figure 4 were determined from this formula, and are in agreement with the fluctuations observed in figure 5. In a Debye dielectric, the relaxation time τ_M is related to the Debye relaxation time τ_D (which is independent of boundary conditions) by [26]

$$\tau_M = \frac{2\epsilon' + 1}{2\epsilon' + \epsilon} \tau_D. \quad (14)$$

Inserting (14) into (13), we see that larger values of ϵ' will lead to smaller uncertainties in the dielectric constant. This explains the faster convergence of ϵ observed when using metallic boundary conditions [5, 22].

According to the present analysis, the slow convergence of ϵ , as determined from the fluctuation formula, is due to the large value of the Debye dielectric relaxation time [8] and the rather broad distribution $P(g)$. Moreover, the uncertainties in ϵ are independent of system size, as long as it is macroscopic. In large systems, it may therefore be favourable to determine ϵ from correlation functions rather than from the fluctuation formula.

4. Structure

4.1. The pair distribution function

The pair distribution function $h(1, 2) = h(\mathbf{r}, \boldsymbol{\mu}_1, \boldsymbol{\mu}_2)$ of the infinite system can be expanded in rotational invariants [27]:

$$h(1, 2) = h^{000}(r) + h^{110}(r)\Phi^{110}(1, 2) + h^{112}(r)\Phi^{112}(1, 2) + \dots,$$

where

$$\Phi^{110}(1, 2) = \hat{\boldsymbol{\mu}}_1 \cdot \hat{\boldsymbol{\mu}}_2, \quad (15)$$

$$\Phi^{112}(1, 2) = 3(\hat{\boldsymbol{\mu}}_1 \cdot \hat{\mathbf{r}})(\hat{\boldsymbol{\mu}}_2 \cdot \hat{\mathbf{r}}) - \hat{\boldsymbol{\mu}}_1 \cdot \hat{\boldsymbol{\mu}}_2. \quad (16)$$

The functions $\Phi^{h^l l}$ form an orthogonal basis for the angular dependence of $h(1, 2)$. The first projections are

$$h^{000}(r) = \langle h(1, 2) \rangle_{\boldsymbol{\mu}_1, \boldsymbol{\mu}_2} = g(r) - 1, \quad (17)$$

$$h^{110}(r) = 3 \langle h(1, 2) \Phi^{110}(1, 2) \rangle_{\boldsymbol{\mu}_1, \boldsymbol{\mu}_2}, \quad (18)$$

$$h^{112}(r) = \frac{3}{2} \langle h(1, 2) \Phi^{112}(1, 2) \rangle_{\boldsymbol{\mu}_1, \boldsymbol{\mu}_2}, \quad (19)$$

where $\langle \dots \rangle_{\boldsymbol{\mu}} = \int \dots d\Omega_{\boldsymbol{\mu}}/4\pi$ denotes an unweighted angular average over the orientations of $\boldsymbol{\mu}$.

Plots of $h^{000}(r)$ and $h^{112}(r)$ are shown in figure 6 for three elongations d of the dipole. As d is increased, the stronger multipolar moments carried by the molecules lead to a slight reduction of the fluid structure as measured by the centre-to-centre distribution $g(r)$, but more orientational order, as measured by the projections $h^{112}(r)$ and $h^{110}(r)$ (the latter projection, not shown in the figure, closely resembles $h^{112}(r)$).

The projection $h^{112}(r)$ is related to the dielectric constant of the fluid by the formula

$$\lim_{r \rightarrow \infty} r^3 h^{112}(r) = \frac{(\epsilon - 1)^2}{\epsilon} \frac{1}{4\pi\rho y}, \quad (20)$$

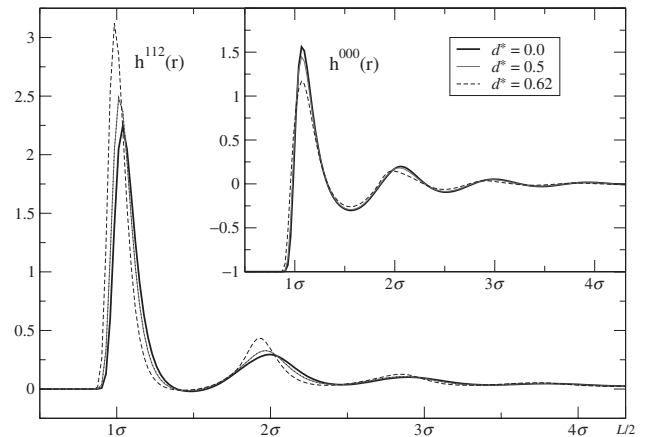


Figure 6. Projections $h^{000}(r)$ and $h^{112}(r)$ of the pair correlation function for three values of $d^* = d/\sigma$.

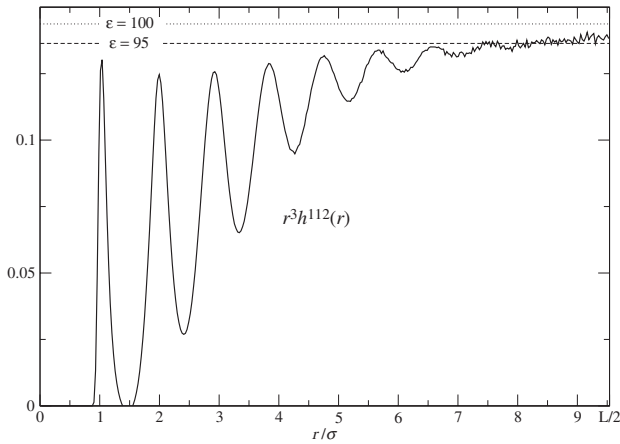


Figure 7. Convergence of $r^3 h^{112}(r)$ at large distances towards the limit (20). Data from a 6 ns long simulation of a system of 5555 molecules ($\rho^* = 0.82$, $T^* = 1.15$, $\mu^* = 1.82$, $d^* = 0.5$).

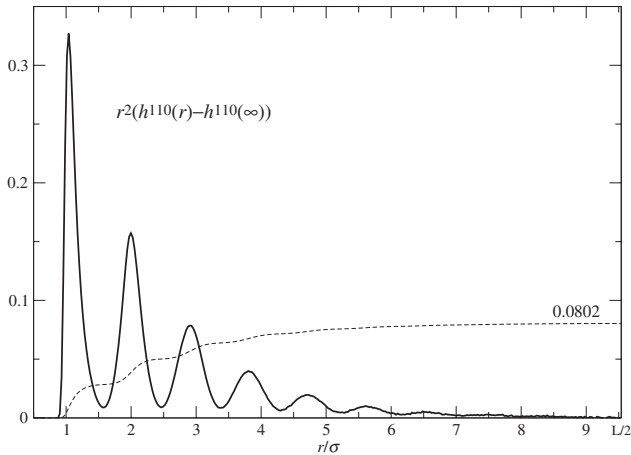


Figure 8. The function $r^2(h^{110}(r) - h^{110}(\infty))$ and its integral (dashed line). Same system as in figure 7.

first derived by Nienhuis and Deutch [28]. A 512-molecule system with a half box size of $L/2\sigma = 4.3$ is too small to reach the asymptotic limit (20). The results for the correlation function shown in figures 7–10 were hence obtained using a larger system (simulation of 5555 molecules during 6 ns) under the same conditions ($\rho^* = 0.82$, $T^* = 1.15$, $\mu^* = 1.82$, $d = \sigma/2$, $\epsilon' = \infty$). Now $L/2\sigma = 9.55$, and figure 7 shows that $r^3 h^{112}(r)$ does reach the asymptotic value (20) at a distance $r \simeq 7\sigma$, as in the case of point dipoles [18]. In [18], it was observed that $r^3 h^{112}(r)$ drops sharply for r greater than $L/2$, even when the reduced size of the volume element is properly taken into account in the normalization. In a system with long range forces, care must be exercised in the interpretation of correlation functions at distances larger than half the box length (since the Ewald potential differs strongly from the Coulomb potential

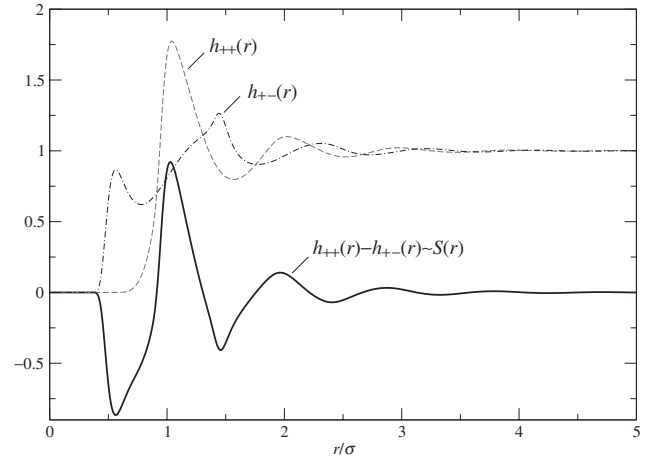


Figure 9. Site-site distribution functions. Same system as in figure 7.

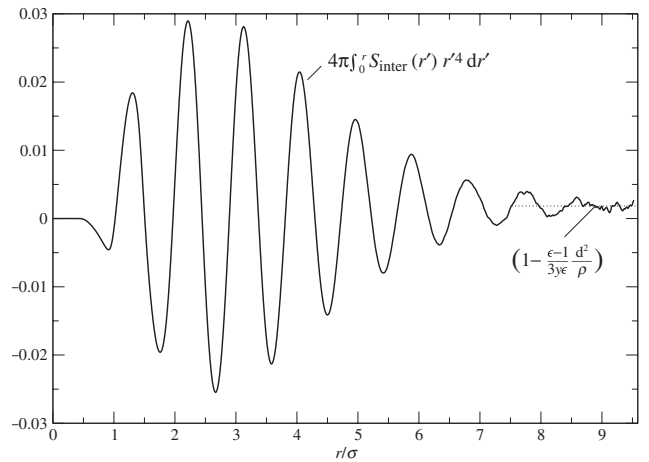


Figure 10. Integration of the second moment of $S_{\text{inter}}(r)$.

at these distances). Caillol analysed this problem carefully, and derived a formula for the asymptotic behaviour of $h^{112}(r)$ valid for distances up to $\sqrt{2}L/2$ [29]. Estimations of the dielectric constant from equation (20) become more accurate when the size of the system is increased, contrary to estimations based on the fluctuation formula.

The projection $h^{110}(r)$ is also related to the dielectric constant, since the fluctuation formula (5) can be written in the Kirkwood form[†]

$$\frac{(\epsilon - 1)(2\epsilon' + 1)}{2\epsilon' + \epsilon} = 3y \left(1 + \frac{4\pi\rho}{3} \int_0^\infty h_{\epsilon'}^{110}(r) r^2 dr \right). \quad (21)$$

[†] For a cubic simulation cell, the upper limit in the integral becomes $3^{1/2}L/2$.

Since the LHS of equation (21) depends on ϵ' , the projection $h^{110}(r)$ must also be sensitive to this boundary condition, whence the introduction of a subscript ϵ' . Figure 8 shows a plot of $r^2 h_\infty^{110}(r)$, and the integral of this function, for the same system as in figure 7. The correlations extend up to $r \simeq 7\sigma$, just as in the case of $h^{112}(r)$. This distance corresponds to the scale beyond which the fluid behaves as a continuum dielectric and obeys the equations of macroscopic electrostatics.

Though formula (21) is equivalent to (5), it is worthwhile to discuss how the pair correlation function depends on the dielectric constant of the external medium. This problem has been addressed in [28] (see also the perturbation theory presented in [5]); here, we hope to give a clear and concise answer to the above question, using simple physical arguments to justify the formulas.

In a spherical sample, $h_\epsilon^{110}(r)$ is in fact the only projection, among all the $h_\epsilon^{l_1 l_2 l}$, to be strongly affected by the boundary condition ϵ' . This is due to the surface term in the Hamiltonian (3), which corresponds to an interaction energy between two molecules

$$\frac{4\pi}{2\epsilon' + 1} \frac{\boldsymbol{\mu}_1 \cdot \boldsymbol{\mu}_2}{V}, \quad (22)$$

which has the angular dependence of $\Phi^{110}(1, 2)$.

As the interaction (22) is independent of the distance between the molecules, $h_\epsilon^{110}(r)$ does not decay in general to zero at infinity, but rather to an ϵ' -dependent constant. We will prove below that this constant is

$$\lim_{r \rightarrow \infty} h_\epsilon^{110}(r) = \frac{2(\epsilon - 1)^2}{V} \frac{\epsilon' - \epsilon}{3\rho y \epsilon} \frac{\epsilon' - \epsilon}{2\epsilon' + \epsilon} \quad (23)$$

in the spherical geometry [5, 28, 29]. The constant (23) vanishes only when using the boundary condition $\epsilon' = \epsilon$, which mimics an infinite sample, or in the thermodynamic limit $V \rightarrow \infty$ (which is never reached in simulations). The limit (23) is achieved in practice at distances large compared to the decay length of $h^{110}(r)$, but small compared to the size of the system.

The fact that $h_\epsilon^{110}(r)$ contains the $\mathcal{O}(1/V)$ constant contribution (23) at large distances ensures that Kirkwood formula (21) gives consistent results for different boundary conditions. Indeed, when $h_\epsilon^{110}(r)$ is integrated over the volume $V = 4\pi R^3/3$ of a large sample, as in the RHS of equation (21), the constant (23) gives a finite contribution to the integral that is precisely what is required to match the ϵ' -dependence of the LHS of the equation. In other words, equations (22) and (23) imply that

$$4\pi \int_0^R h_\epsilon^{110}(r) r^2 dr = 4\pi \int_0^R h_\epsilon^{110}(r) r^2 dr + V h_\epsilon^{110}(\infty),$$

when the samples are large enough (i.e. in the limit $R \rightarrow \infty$). When this identity is inserted into Kirkwood formula (21), it is immediately clear that the predicted dielectric constant is independent of ϵ' .

In order to prove equation (23) with simple physical arguments, we need to recall two basic results from the statistical mechanics of polar liquids. The first result is the expression of the density $\rho(\mathbf{r}, \boldsymbol{\mu})$ of molecules at \mathbf{r} with orientation $\boldsymbol{\mu}$ in a polarized sample permeated by a macroscopic field $\mathbf{E}(\mathbf{r})$: [30]

$$\rho(\mathbf{r}, \boldsymbol{\mu}) = \frac{\rho}{4\pi} \left(1 + \frac{\epsilon - 1}{3y} \beta \boldsymbol{\mu} \cdot \mathbf{E}(\mathbf{r}) \right) + \mathcal{O}(E^2) \quad (24)$$

(y is defined after equation (6)). This formula is consistent with the constitutive relation $\mathbf{P}(\mathbf{r}) = (\epsilon - 1)/(4\pi)\mathbf{E}(\mathbf{r})$ of macroscopic electrostatics, since the average polarization density in the fluid is by definition $\mathbf{P}(\mathbf{r}) = \int \rho(\mathbf{r}, \boldsymbol{\mu}) \boldsymbol{\mu} d\Omega_\mu$.

The second result we need is the expression of the effective dipole moment $\boldsymbol{\mu}^{\text{eff}}$ of a polar molecule held fixed in a polar liquid ($\boldsymbol{\mu}^{\text{eff}}$ is defined as $\boldsymbol{\mu}$, the dipole moment of the fixed molecule, plus the total dipole moment of the screening cloud around $\boldsymbol{\mu}$). One may first think naively that $\boldsymbol{\mu}^{\text{eff}} = \boldsymbol{\mu}/\epsilon$: the fluid would screen the dipole according to its dielectric constant. But this would be treating the polar fluid as a dielectric continuum everywhere, including in the interior of the fixed molecule, which is obviously wrong. An exact statistical mechanical calculation shows that the right answer is [31]

$$\boldsymbol{\mu}^{\text{eff}} = \frac{\epsilon - 1}{3y\epsilon} \boldsymbol{\mu}. \quad (25)$$

(The expression $(\epsilon - 1)/3y\epsilon$ can itself be interpreted as being composed of a factor $(\epsilon - 1)/3y$ arising from local correlations around $\boldsymbol{\mu}$, times the expected factor $1/\epsilon$ due to screening by distant molecules). With these two results in mind, we can now understand easily formulas (20), (22) and (23).

The result (20) for the large-distance behaviour of the pair correlation function $h(1, 2)$ can be seen as a straightforward consequence of the screening effect (25). By definition of the distribution functions, the density of molecules at \mathbf{r}_2 with orientation $\boldsymbol{\mu}_2$, when a molecule is known to be located at $1 = (\mathbf{r}_1, \boldsymbol{\mu}_1)$ is

$$\rho(2|1) = \frac{\rho(2, 1)}{\rho(1)} = \frac{\rho}{4\pi} (1 + h(1, 2)). \quad (26)$$

From (25), the electric field due to the fixed molecule $\boldsymbol{\mu}_1$ is equivalent, at large distances $\mathbf{r}_{12} = \mathbf{r}_2 - \mathbf{r}_1$, to that of a renormalized dipole moment $\boldsymbol{\mu}_1^{\text{eff}}$. This dipolar field

$-\nabla_2(\boldsymbol{\mu}_1^{\text{eff}} \cdot \nabla_1)|\mathbf{r}_{12}|^{-1}$ is locally uniform and weak, so we can apply the linear response result (24). Using (24) and (25), we find that

$$\rho(2|1) \underset{|\mathbf{r}_{12}| \rightarrow \infty}{\sim} \frac{\rho}{4\pi} \left(1 - \frac{(\epsilon - 1)^2}{9y^2\epsilon} \beta v_{\text{dip}}(1, 2) \right), \quad (27)$$

where $v_{\text{dip}}(1, 2) = (\boldsymbol{\mu}_1 \cdot \nabla_1)(\boldsymbol{\mu}_2 \cdot \nabla_2)|\mathbf{r}_{12}|^{-1}$ is the dipolar potential, and we assume an infinitely extended sample. Comparing (26) and (27), we obtain the asymptotic behaviour of the pair correlation function:

$$h(1, 2) \underset{|\mathbf{r}_{12}| \rightarrow \infty}{\sim} \frac{(\epsilon - 1)^2}{9y^2\epsilon} (-\beta v_{\text{dip}}(1, 2)). \quad (28)$$

The result (20) follows then upon inserting (28) into (19).

Formula (23) can be interpreted in a similar way, namely as arising from the interaction of a molecule with the reaction field produced by the screened dipole moment of another molecule. We recall from macroscopic electrostatics that a dipole $\boldsymbol{\mu}_1$ at the centre of a spherical sample of radius R and dielectric constant ϵ , surrounded by a dielectric medium ϵ' , produces a uniform reaction field

$$\mathbf{E}_R^{[\epsilon, \epsilon']}(\boldsymbol{\mu}_1) = \frac{2}{\epsilon} \frac{\epsilon' - \epsilon}{2\epsilon' + \epsilon} \frac{\boldsymbol{\mu}_1}{R^3} \quad (29)$$

inside the sample, because of the surface charge density induced at the dielectric discontinuity [32]. In a finite spherical sample, a molecule at a position \mathbf{r}_2 far enough from $\boldsymbol{\mu}_1$ —so that it does not disturb the screening cloud around it—will interact therefore not only with the dipolar field of $\boldsymbol{\mu}_1^{\text{eff}}$, as in (27), but also with the reaction field $\mathbf{E}_R(\boldsymbol{\mu}_1^{\text{eff}})$ produced by the screened dipole moment of this molecule. From (24), a term

$$\frac{\rho}{4\pi} \cdot \frac{\epsilon - 1}{3y} \beta \boldsymbol{\mu}_2 \cdot \mathbf{E}_R^{[\epsilon, \epsilon']}(\boldsymbol{\mu}_1^{\text{eff}}), \quad (30)$$

must hence be added to (27) in a finite spherical sample. The pair correlation at large distances, equation (28), includes then the additional contribution

$$\frac{4\pi}{3V} \frac{2(\epsilon - 1)^2}{9y^2\epsilon} \frac{\epsilon' - \epsilon}{2\epsilon' + \epsilon} \beta \boldsymbol{\mu}_2 \cdot \boldsymbol{\mu}_1, \quad (31)$$

where we used (29), (25) and $V = 4\pi R^3/3$. Formula (23) follows now from projecting (31) onto $\Phi^{110}(1, 2) = \hat{\boldsymbol{\mu}}_1 \cdot \hat{\boldsymbol{\mu}}_2$ according to (18).

We conclude this discussion by noting that the interaction energy (22) used in the simulations, or equivalently the surface term in the Hamiltonian (3), can also be interpreted in terms of a reaction field effect. Indeed, each polar molecule in the sample will create a

reaction field, acting on itself and on all other molecules, that are given by equation (29) with $\epsilon = 1$. Since the Ewald sums (4) give the electrostatic energy between the molecules in the case of a sample surrounded by a metal ($\epsilon' = \infty$), the correction to this energy to be used in the Hamiltonian of a spherical system with boundary condition ϵ' is

$$\frac{1}{2} \sum_{i,j=1}^N (-\boldsymbol{\mu}_i) \cdot \left[\mathbf{E}_R^{[1, \epsilon']}(\boldsymbol{\mu}_j) - \mathbf{E}_R^{[1, \infty]}(\boldsymbol{\mu}_j) \right] = \frac{2\pi \mathbf{M}^2}{(2\epsilon' + 1)v}, \quad (32)$$

in agreement with (3).

4.2 Site–site correlations

Contrary to the point dipolar fluid model, the present model with extended dipoles has well-defined site–site distribution functions $h_{++}(r) = h_{--}(r)$ and $h_{+-}(r)$ [33]. From these we get the charge–charge correlation function $S(r) = S_{\text{intra}}(r) + S_{\text{inter}}(r)$, where

$$S_{\text{inter}}(r) = 2q^2 \rho^2 (h_{++}(r) - h_{+-}(r)) \quad (33)$$

describes the intermolecular correlations, while

$$S_{\text{intra}}(r) = 2q^2 \rho \delta(\mathbf{r}) - 2q^2 \rho \frac{\delta(|\mathbf{r}| - d)}{4\pi d^2} \quad (34)$$

is the intramolecular correlation function for a molecule with a rigid dipole of extension d . The charge–charge correlation is of special interest, because it satisfies the two sum rules [34]:

$$\text{neutrality : } \int S(r) d^3\mathbf{r} = 0, \quad (35)$$

$$\text{Stillinger–Lovett : } \frac{1}{\epsilon} = 1 + \frac{2\pi\beta}{3} \int d^3\mathbf{r} r^2 S(r). \quad (36)$$

The site–site correlation functions and $S(r)$ are shown on figure 9 for $d = \sigma/2$. The charge neutrality sum rule is found to be accurately satisfied:

$$\rho \int_0^\infty (h_{++}(r) - h_{+-}(r)) r^2 dr \simeq 8.8 \times 10^{-5}. \quad (37)$$

The Stillinger–Lovett sum rule allows in principle the determination of the dielectric constant from $S(r)$, but this route is not practicable in a computer simulation, because of the unfavourable ratio $(1 - \epsilon)/\epsilon$ which saturates for large ϵ , and also because it is difficult to determine the second moment of $S_{\text{inter}}(r)$ accurately. Figure 10 shows, however, that equation (36) is satisfied within the uncertainties of our data.

5. Orientational order

When the molecular dipole has an extension greater than $d \simeq 0.64\sigma$, the simulations show spontaneous formation of orientationally ordered phases, starting from random initial configurations. At the state point under consideration ($\rho^* = 0.82$, $T^* = 1.15$), we observed phase coexistence between a dense liquid crystal and a very dilute gas. In order to deal with pure phases, we performed simulations at constant pressure ($p^* = p\sigma^3/u = 0.22$), rather than constant volume, for $d \geq 0.62\sigma$.

The occurrence of orientational order was monitored by computing two order parameters. The rank-one order parameter P_1 is defined as

$$P_1 = \frac{\langle M_{\parallel} \rangle}{N\mu}, \quad (38)$$

where $M_{\parallel} \equiv \mathbf{M} \cdot \hat{\mathbf{n}}$ is the projection of the total dipole moment along the director \mathbf{n} ($P_1 = 1$ for a completely polarized system). The second-rank order parameter P_2 is the largest eigenvalue of the matrix

$$Q_{\alpha\beta} = \frac{1}{N\mu^2} \left\langle \sum_{i=1}^N \frac{1}{2} (3\mu_i^\alpha \mu_i^\beta - \mu^2 \delta_{\alpha\beta}) \right\rangle, \quad (39)$$

where μ_i^α is the α component of the vector $\boldsymbol{\mu}_i$. The corresponding eigenvector \mathbf{n} is the director. $P_2 = 1$ when all dipoles are oriented parallel to \mathbf{n} or $-\mathbf{n}$.

Table 2 lists our results for these order parameters, as well as for the dielectric tensor $\boldsymbol{\epsilon} = (\epsilon_{\parallel}, \epsilon_{\perp})$. In a liquid crystal with director \mathbf{n} , the latter is determined by the

following generalization of equation (6):

$$\epsilon_{\parallel} = 1 + y \frac{\langle M_{\parallel}^2 \rangle - \langle M_{\parallel} \rangle^2}{N\mu^2}, \quad (40)$$

and a similar equation for ϵ_{\perp} in terms of the perpendicular fluctuations $(\langle \mathbf{M}_{\perp}^2 \rangle - \langle \mathbf{M}_{\perp} \rangle^2)/N\mu^2$.

When d is increased above the critical distance $d_c \simeq 0.63\sigma$, the order parameter P_2 jumps from essentially zero to about almost one, indicating a first-order transition to a highly orientationally ordered phase. Figure 11 provides snapshots of the simulation cell for $d = 0.64\sigma$. It is clear from the snapshots that the molecules are associated into columns, composed of chains of dipoles oriented head-to-tail. These columns are all parallel to the director, and are arranged in a hexagonal lattice in the perpendicular plane. The simulations for $d > 0.64\sigma$ yielded similar liquid crystal phases with columnar order, each with a different

Table 2. Constant pressure simulations of a Stockmayer fluid at $\rho^* = 0.22$, $T^* = 1.15$ and $\mu^* = 1.82$. Data from 8 ns long simulations of 512 molecules, collected after an equilibration period that lasted up to 10 ns. For $d \geq 0.64\sigma$, the system is a ferro-electric liquid crystal with columnar order. Uncertainties in ϵ_{\parallel} and ϵ_{\perp} are about ± 0.01 and ± 0.02 respectively.

d/σ	$\langle \rho^* \rangle$	P_1	P_2	ϵ_{\parallel}	ϵ_{\perp}
0.62	0.80	0.08	0.07	$\epsilon = 103.8(\pm 4)$	
0.63	0.80	0.09	0.08	$\epsilon = 112.6(\pm 5)$	
0.64	0.95	0.97	0.91	1.16	1.46
0.65	0.98	0.66	0.91	1.28	1.56
0.66	1.03	0.98	0.94	1.02	1.43

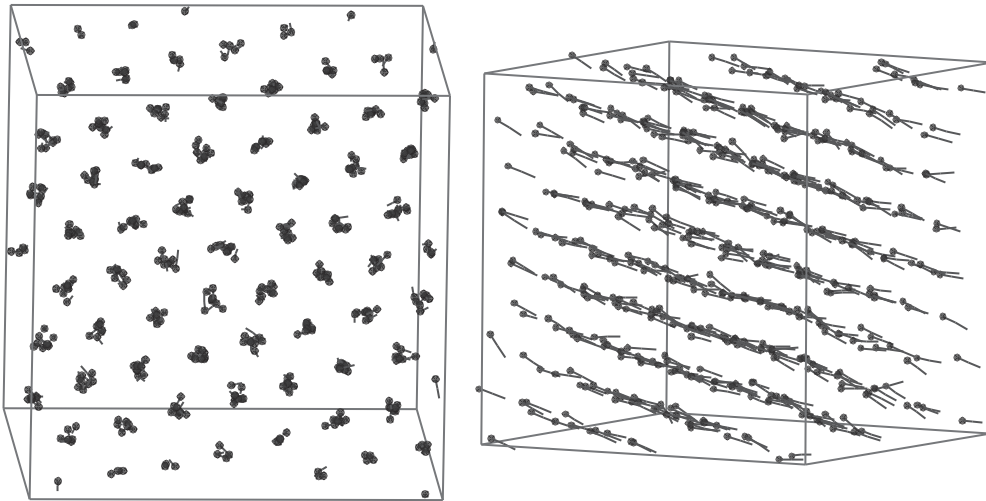


Figure 11. Snapshots of the simulation cell of the Stockmayer fluid in the columnar phase. The hexagonal lattice in the plane orthogonal to the director is apparent in the first snapshot. The dipoles are represented by a line joining the minus charge (shown as a small bead) to the plus charge.

orientation of the director. The system shows strong spatial correlations in the direction of the director, but it is still fluid in that direction, as indicated by the mean-square displacement of the molecules. The latter increases indeed linearly with time, with a diffusion constant of about $D_{\parallel} \simeq 0.09 \times 10^{-5} \text{ cm}^2 \text{ s}^{-1}$.

In some runs (not listed in table 2), the system formed two liquid crystal domains characterized by different orientations of the director. As the transition to a single domain is expected to occur on a time scale much larger than our simulation time (8 ns), since it requires the collective motion of many molecules, we included in table 2 only results from runs where a single domain formed spontaneously in less than 10 ns. Most runs yielded fully polarized liquid crystals (P_1 close to 1). It is likely that the lower value of P_1 measured in the case $d = 0.65\sigma$ is due to insufficient sampling of phase space: the probability of a column inverting its orientation during our simulation time is indeed very small.

As the column configuration is energetically more favourable for extended than for point dipoles (see figure 2), it is not surprising that liquid crystal columnar phases form at a much lower dipolar coupling constant $\lambda = \mu^{*2}/T^*$ than previously reported for point dipolar fluid models; here $\lambda \sim 2.9$, while columnar phases were observed in the dipolar soft sphere fluid at $\lambda = 9$, and in the dipolar hard sphere fluid at $\lambda = 6.25$ [9, 35]. A nematic ferroelectric liquid phase has been identified in the Stockmayer model at $\lambda \simeq 4$ (a columnar phase has not been seen previously in this model to our knowledge) [36, 37]. The hexagonal lattice arrangement found here is to be contrasted with the square lattice reported in [35].

6. Conclusion

We have extended the considerable body of earlier work on dipolar fluids by replacing the usual point dipole on spherical molecules by physically more relevant extended dipoles obtained by placing two opposite charges symmetrically with respect to the centre. The structural, dielectric and dynamical behaviour was monitored as the spacing d of the charges was increased, keeping the total dipole moment $\mu = qd$ fixed. Periodic boundary conditions were used with proper Ewald summations of the Coulombic interactions within an infinitely large sphere bounded by a dielectric medium of permittivity ϵ' . The key findings are the following:

- a) Runs of several nanoseconds, longer than in most previous studies, were required to obtain estimates of the dielectric constant ϵ within about 2% using the standard fluctuation formula (5).

A careful error analysis shows that ‘metallic’ boundary conditions (where $\epsilon' = \infty$ at infinity) yield optimal estimates of ϵ .

- b) The values of ϵ deduced from the h^{112} and h^{110} correlation functions agree with the fluctuation results within statistical errors, provided a sufficiently large simulation cell is used to obtain proper estimates of the asymptotic behaviour of these correlation functions. The strong influence of the boundary condition ϵ' on the projection $h^{110}(r)$ arises from the interaction of the polar molecules with the reaction field to the dielectric discontinuity between the fluid and the external medium ϵ' . When $\epsilon' \neq \epsilon$, $h^{110}(r)$ does not decay to zero at large distances, but rather to a finite constant of order $1/V$ [5, 28, 29]. The value of this constant (equation (23)) was derived using simple physical arguments based on macroscopic electrostatics and linear response theory.
- c) ϵ has a non-trivial dependence on the ratio $d^* = d/\sigma$. Up to $d^* \simeq 0.25$, ϵ agrees with the point dipole result within statistical uncertainties, thus illustrating the practical usefulness of the point dipole limit. For $d^* \gtrsim 0.3$, ϵ drops to a minimum value roughly 6% below the point dipole result when $d^* \simeq 0.55$. When d^* is further increased, ϵ increases sharply and reaches a maximum at $d^* \simeq 0.6$.
- d) For still larger extensions d^* , the system is seen to undergo a transition, at constant pressure, to an orientationally ordered state similar to a columnar phase with a hexagonal ordering in the plane orthogonal to the director. This phase is characterized by large values of the usual orientational order parameters P_1 and P_2 . At the same time the dielectric tensor becomes anisotropic, and the mean dielectric constant is very low ($\epsilon \simeq 1.4$), signalling the strong suppression of dipole moment fluctuations. The transition to the columnar phase occurs at a value of the dipole moment well below that required to observe the transition with point dipoles [9, 35].
- e) The dynamics, characterized by the relaxation times τ_M and τ_{μ} of the total and individual dipole moments, as well as by the self-diffusion constant D , slows down very significantly as d^* increases, due to the enhanced tendency of the system to form parallel strings, which eventually lead to the columnar phase. In the latter, the diffusion coefficient D_{\parallel} parallel to the director is about two orders of magnitude smaller than D in the isotropic phase, but still substantial, showing that the system behaves like a one-dimensional fluid.

The present results are for a single high-density $\rho^* = 0.82$, and a single pressure in the anisotropic phase ($p^* = 0.22$, corresponding to $\langle \rho^* \rangle \simeq 1$). Clearly more work is needed to be able to map out a complete phase diagram of the Stockmayer fluid, in view of the additional variable d^* . The present work illustrates the strengths and deficiencies of the point-dipole model. Many simple molecular systems fall in the region $d^* \simeq 0.5$, where the deviations from point dipole behaviour begin to be substantial.

The authors thank Joachim Dzubiella, Reimar Finken, Michael Klein and Mark Miller for fruitful discussions. The financial support of the Swiss National Science Foundation is also gratefully acknowledged.

References

- [1] ONSAGER, L., 1936, *J. Am. chem. Soc.*, **58**, 1486.
- [2] KIRKWOOD, J., 1939, *J. chem. Phys.*, **7**, 911.
- [3] STELL, G., PATEY, G. N., and HØYE, J. S., 1981, *Adv. Chem. Phys.*, **48**, 183; MADDEN, P. A., and KIVELSON, D., 1984, *Adv. Chem. Phys.*, **56**, 467.
- [4] PATEY, G. N., LEVESQUE, D., and WEIS, J. J., 1982, *Molec. Phys.*, **45**, 733.
- [5] DE LEEUW, S. W., PERRAM, J. W., and SMITH, E. R., 1980, *Proc. R. Soc. Lond. A*, **373**, 27; *ibid.*, **373**, 57; *ibid.*, **388**, 177.
- [6] NEUMANN, M., 1983, *Molec. Phys.*, **50**, 841.
- [7] KUSALIK, P. G., 1990, *J. chem. Phys.*, **93**, 3520.
- [8] KURTOVIĆ, Z., MARCHI, M., and CHANDLER, D., 1993, *Molec. Phys.*, **78**, 1155.
- [9] WEI, D., and PATEY, G. N., 1992, *Phys. Rev. Lett.*, **68**, 2043.
- [10] WEIS, J. J., and LEVESQUE, D., 1993, *Phys. Rev. E*, **48**, 3728.
- [11] GROH, B., and DIETRICH, S., 1994, *Phys. Rev. Lett.*, **72**, 2422.
- [12] VAN LEEUWEN, M. E., and SMIT, B., 1993, *Phys. Rev. Lett.*, **71**, 3991.
- [13] KLEIN, M. L., and McDONALD, I. R., 1979, *J. chem. Phys.*, **71**, 298.
- [14] WEI, D., 1995, *Molec. Crystal Liq. Crystal*, **269**, 89.
- [15] CICCOTTI, G., FERRARIO, M., HYNES, J. T., and KAPRAL, R., 1989, *Chem. Phys.*, **129**, 241.
- [16] HERTZNER, A. W., SCHOEN, M., and MORGNER, H., 1991, *Molec. Phys.*, **73**, 1011.
- [17] JACKSON, J. D., 1998, *Classical Electrodynamics*, 3rd edn (New York: John Wiley and Sons).
- [18] KUSALIK, P. G., 1991, *Molec. Phys.*, **73**, 1349.
- [19] ESSMAN, U., PERELA, L., BERKOWITZ, M. L., DARDEN, T., LEE, H., and PEDERSEN, L. G., 1999, *J. chem. Phys.*, **110**, 8577.
- [20] LINDAHL, E., HESS, B., and VAN DER SPOEL, D., 2001, *J. molec. Mod.*, **7**, 306 (<http://www.gromacs.org>).
- [21] FRENKEL, D., and SMIT, B., 2002, *Understanding Molecular Simulation*, 2nd edn (London: Academic Press).
- [22] WANG, Z., HOLM, C., and MÜLLER, H. W., 2003, *J. chem. Phys.*, **119**, 379.
- [23] KUSALIK, P. G., MANDY, M. E., and SVISHCHEV, I. M., 1994, *J. chem. Phys.*, **100**, 7654.
- [24] HÖCHTL, P., BORESCH, S., BITOMSKY, W., and STEINHAUSER, O., 1998, *J. chem. Phys.*, **109**, 4927.
- [25] KUSALIK, P. G., 1993, *Molec. Phys.*, **80**, 225.
- [26] NEUMANN, M., and STEINHAUSER, O., 1983, *Chem. Phys. Lett.*, **102**, 508.
- [27] GRAY, C. G., and GUBBINS, K. E., 1984, *Theory of Molecular Fluids*, Vol. 1 (Oxford: Clarendon Press).
- [28] NIENHUIS, G., and DEUTCH, J. M., 1971, *J. chem. Phys.*, **55**, 4213.
- [29] CAILLOL, J. M., 1992, *J. chem. Phys.*, **96**, 7039.
- [30] ALASTUEY, A., and BALLENEGGER, V., 2000, *Physica A*, **279**, 268.
- [31] FINKEN, R., BALLENEGGER, V., and HANSEN, J.-P., 2003, *Molec. Phys.*, **101**, 2559.
- [32] FRÖHLICH, H., 1949, *Theory of Dielectrics* (Oxford: Oxford University Press).
- [33] HANSEN, J.-P., and McDONALD, I. R., 1986, *Theory of Simple Liquids*, 2nd edn (London: Academic Press).
- [34] MARTIN, PH. A., 1988, *Rev. Mod. Phys.*, **60**, 1075.
- [35] WEIS, J. J., LEVESQUE, D., and ZARRAGOICOECHEA, G. J., 1992, *Phys. Rev. Lett.*, **69**, 913.
- [36] STEVENS, M. J., and GREST, G. S., 1995, *Phys. Rev. E*, **51**, 5976.
- [37] GAO, G. T., and ZENG, X. C., 2000, *Phys. Rev. E*, **61**, R2188.